Plant Direct

WILEY

American Society of Plant Biologists SEB SOCIETY FOR EXPERIMENTAL BIOLOGY

RESEARCH ARTICLE OPEN ACCESS

PECTIN METHYLESTERASE51 Affects Stomatal Dimensions, Rosette Area, and Root Length in *Arabidopsis thaliana*

Angelica L. Dunham | Chetana Tamadaddi | Rayna Marshall | Charles T. Anderson

Department of Biology, The Pennsylvania State University, University Park, Pennsylvania, USA

Correspondence: Charles T. Anderson (cta3@psu.edu)

Received: 15 April 2024 | **Revised:** 25 March 2025 | **Accepted:** 26 March 2025

Funding: This work was supported by National Science Foundation (NSF) under grant MCB-2015943/2015947.

Keywords: *Arabidopsis thaliana* | guard cell morphogenesis | pectin methylesterase | stomatal function | stomatal guard cells

ABSTRACT

Pectins are abundant in the cell walls of eudicot plants and have been implicated in determining the development and biomechanics of stomatal guard cells, which expand and contract dynamically to open and close stomatal pores on the plant surface, modulating photosynthesis and water transport. Pectic homogalacturonan is delivered to the cell wall in a methylesterified form but can be demethylesterified in the wall by pectin methylesterases, increasing both its ability to form crosslinks via calcium and its susceptibility to degradation by endogenous pectinases. Although a few pectin methylesterases have been implicated in stomatal development and function, this large family of proteins has not been fully characterized with respect to how they modulate stomatal guard cells. Here, we characterized the function of PECTIN METHYLESTERASE51 (*PME51*), a pectin methylesterase–encoding gene that is expressed in developing guard cells, in stomatal morphogenesis in seedlings and adult plants of *Arabidopsis thaliana*. Overexpressing *PME51* led to smaller adult plants with smaller stomatal complexes and subtle changes in initial responses to opening and closure stimuli, whereas knocking out *PME51* resulted in smaller stomatal complexes and longer roots in seedlings. We observed changes in pectin labeling in knockout and overexpression plants that imply a specific function for PME51 in modulating the degree of methylesterification for homogalacturonan. Together, these findings expand our understanding of how pectin modification by pectin methylesterases affects the development and function of stomatal guard cells, which must maintain a balance of strength and flexibility to optimize plant growth.

1 | Introduction

Stomata are pores in the plant epidermis that are important for regulating CO_2 uptake and water movement in plants and play an important role in photosynthesis and transpiration. Stomatal conductance is controlled by an array of hormones and signaling cascades that alter turgor pressure in the guard cells that flank stomatal pores (Liu et al. 2022). Environmental factors like CO_2, temperature, and water availability can also affect stomatal opening and closing (Wu et al. 2017). The optimal modulation of stomatal conductance relies on the ability of the plant to open its stomatal pores fast enough to enable CO_2 entry for efficient photosynthesis but close fast enough to minimize unnecessary water loss (Drake et al. 2013). These qualities are especially important in plants that grow under water limiting conditions: If the plant can open and close its stomata fast enough, the plant

Angelica L. Dunham and Chetana Tamadaddi contributed equally.

should be able to reduce water loss and will be better equipped to survive in drought conditions (Kim et al. 2010).

Like almost all plant cells, stomatal guard cells are encased in polysaccharide-based cell walls, but the walls of guard cells must remain both strong enough to withstand the high turgor pressures generated in these cells and flexible enough to allow for guard cell expansion and contraction during stomatal opening and closure, respectively (Keynia et al. 2023). Pectin, which is one of the most abundant wall polysaccharides in plants, makes up around 50% of the walls of growing cells in *Arabidopsis thaliana* (Zablackis et al. 1995). Pectin is made up of homogalacturonan (HG), which is an unbranched polymer of α-(1–4) linked galacturonic acid (GalA) residues, along with other pectin domains that contain side branches (Harholt et al. 2010). HG is initially synthesized in a high methylesterified state, but once it is delivered to the cell wall, it can be demethylesterified by pectin methylesterases (PMEs). PMEs cleave the methylester group from the C6 position on GalA, releasing methanol and protons to create negatively charged carboxyl groups on GalA residues (Caffall and Mohnen 2009). When HG is demethylesterified, stretches of GalA residues in adjacent HG chains can be crosslinked by calcium ions (Ca^{2+}), which leads to a stiffer cell wall (Limberg et al. 2000; Liners et al. 1989).

A total of 66 open reading frames encoding putative or confirmed PMEs have been annotated in the genome of *A. thaliana*. Among these 66 PMEs, some have been found to function in plant development, stomatal dynamics, abiotic stress responses, and plant immunity (Micheli 2001; Wu et al. 2018). Many PME genes encode PRE-PRO proteins that include PME peptide motifs. The PRE domain consists of a signal peptide and a transmembrane domain and is responsible for the export of PMEs to the cell wall. The PRO region inhibits PME activity and helps prevent the premature demethylesterification of HG (Bosch and Hepler 2006; Wolf et al. 2009). There are two types of PMEs: Type 1 PMEs have 1–3 PRO domains and 2–3 introns, whereas Type 2 PMEs lack PRO domains and are made up of 5–6 introns (Manmohit Kalia 2015; Micheli 2001). *PME51*, the gene we characterize here, encodes a Type 2 PME (Sénéchal et al. 2014).

The characterization of *PME51* is of interest because pectic polymers in the guard cell wall are influential in promoting or slowing stomatal movement (Jones et al. 2003). Guard cell walls in *A. thaliana* contain high levels of demethylesterified HG, suggesting that PMEs might play important roles in stomatal function (Amsbury et al. 2016). *PME6* is highly expressed in guard cells, and *pme6* knockout mutants show decreased stomatal conductance (Amsbury et al. 2016). *PME51* (At5g09760) is also expressed in stomatal guard cells (Hachez et al. 2011). To better understand the function of *PME51*, we characterized its expression through a PME51pro::GUS reporter line and examined knockout (*pme51-1*), overexpression (*PME51-OE*), and complementation (*PME51-comp*) lines for this gene in *A. thaliana*. We observed that *PME51* is widely expressed across the plant and detected differences in rosette area in *pme51-1* and *PME51-OE* plants when compared with Col-0 controls. *pme51-1* seedlings had longer roots compared with Col-0 and *PME51-OE* plants. Stomata in 6-day-old and 3-week-old *pme51-1* plants had smaller pore lengths than Col-0 controls. In 3-week-old *PME51-OE* plants, stomatal pore width, length and area were smaller than Col-0. We also observed subtle changes in abscisic acid (ABA) induced, fusicoccin (FC)-induced, dark-induced, and light-induced stomatal responses across the *PME51* genotypes, implying that stomatal responses and/or wall architecture might be partially influenced by PME51 activity, but that wall architecture and/or other guard cell properties are modulated to compensate for altered *PME51* expression to retain stomatal function.

2 | Methods

2.1 | Transgenic Lines

The *PME51* (At5g09760) coding sequence was amplified from cDNA and cloned into pEarleyGate101 (Earley et al. 2006) to generate a *PME51-OE* construct containing 35S promoter with Gateway cloning. *PME51-comp* was Gateway cloned into pMDC110/GFP-6xHis cassette B with a 2 kb fragment of the native promoter (At5g09760) with coding sequence and no stop codon. Transgenic lines were selected with 60 μg/mL kanamycin on 1% sucrose ½ MS plates. The mutant line *pme51-1* was SALK_069468. Primers used for generating transgene constructs are shown in Table 1.

2.2 | Plant Growth

A. thaliana seeds were sterilized for 20 min in a solution of 30% bleach (v/v) + 0.1% SDS (w/v), washed four times in sterile water, and resuspended in sterile 0.15% agar (w/v). Sterilized seeds were stored in 4°C in the dark for 3–10 days. Seeds were sowed on Murashige and Skoog (MS) plates containing 2.2 g/L MS salts (Caisson Laboratories, North Logan, UT, USA), 0.6 g/L 2-(N-Morpholino) ethanesulfonic acid (MES, Sigma, St Louis, MO, USA), and 0.8% agar (Sigma, St Louis, MO, USA), pH 5.6. Seedlings were grown at 22°C under 24-h light at ~800 photosynthetic photon flux density for 10 days before being transferred to Fafard C2 soil (Griffin Greenhouse) containing Miracle-Gro (The Scotts Company). Plants were grown in 16-h light/8-h dark conditions at 22°C until they were 3-weeks-old.

2.3 | Root Length Measurements

Forty *A. thaliana* seedlings per plate were grown on 1% sucrose ½ MS plates at 22°C under 24-h light. The plate was taken

TABLE 1 | Primers used in this study.

PME51-OE F	TTCCTTAGCTCAGGTTTATGAGC
PME51-OE R	GGTTATGATTAAGAGACAGAAGC
pme51-1 F	TAGATCACGAGCCATGAATCC
pme51-1 R	TTGTAACGCAACTCGTTACCC
PME51-comp F	ATGTCCTCCATTCTCATCCTTCT
PME51-comp R	AGCAGACATCGAAGCCCACT

out of the growth chamber every day on days 3–7 of growth and imaged with a Nikon D5100 DSLR camera. Images were analyzed using FIJI, measuring the length of the root from the cotyledon (marking the top of the root) to the bottom of the root.

2.4 | PI Staining and Measurements of Stomatal Geometry

Six-day-old *A. thaliana* seedlings grown under 24-h light conditions and epidermal peels from 3-week-old *A. thaliana* leaves were placed under light for 2.5 h at 22°C prior to staining. Seedlings were immersed in 0.1% PI (w/v) solution for 15 min in a 12-well plate. For 3-week-old images, an epidermal peel was collected from the abaxial side, and the samples were placed in a 0.1% PI solution for 15 min in a 12-well plate. Samples were mounted on microscope slides with 70 μL of water. Stomata were imaged using a Zeiss Cell Observer SD spinning disk confocal microscope with a 63× oil immersion objective, a 561-nm excitation laser, and a 617/73 emission filter. Images were analyzed in FIJI using Z-project after enhancing contrast to 0.35% pixel saturation.

2.5 | GUS Staining

Tissues of 6-day-old and 3-week-old ProPME51:GUS transgenic *A. thaliana* plants were stained in 50-mM sodium phosphate, pH 7.2, 0.2% (v/v) Triton X-100, and 2-mM X-Gluc in the dark at 37°C overnight. Tissues were then destained with 70% ethanol by shaking overnight until they became clear, and images were collected with a Zeiss Discovery V12 fluorescence dissecting microscope. Epidermal peels of 3-week-old plants were also observed on a Zeiss Cell Observer SD spinning disk confocal microscope using a 63× oil immersion objective.

2.6 | Rosette Area Measurements

Rosette images collected with a Nikon D5100 DSLR camera were processed in FIJI by converting images to a BW color threshold to isolate the rosette foreground from the background. The wand tool in ImageJ was then used to measure the area of the 3-week-old rosettes.

2.7 | Stomatal Dynamics Analysis for 3-Week-Old Plants

To analyze abscisic acid (ABA)–induced stomatal closure, leaves from 3-week-old plants were pre-incubated for 2.5 h in a 12-well plate containing a solution of 20-mM KCl, 1-mM $CaCl_2$, 5-mM MES-KOH, pH 6.15 under light to induce stomatal opening. Solution was pipetted repeatedly to ensure that bubbles were present in the solution. After pre-incubation, epidermal peels were collected from leaves and were incubated in 20-mM KCl, 1-mM $CaCl_2$, 10-mM MES-KOH, pH 6.15 with 50-μM ABA in a 12-well plate to induce stomatal closure. Images were taken on a brightfield epifluorescence microscope with a 63× oil immersion objective. Images were collected from separate leaves every 30 min after the addition of ABA. To analyze fusicoccin (FC)-induced stomatal opening, leaves were pre-incubated for 2.5 h in solution in a 12-well plate covered with aluminum foil containing 50-mM KCl, 0.1-mM $CaCl_2$, 10-mM MES-KOH, pH 6.15 to induce stomatal closure. Solution was pipetted repeatedly to ensure that bubbles were present in the solution. After preincubation, epidermal peels were collected from leaves and were incubated in a solution containing 50-mM KCl, 0.1-mM $CaCl_2$, 10-mM MES-KOH, pH 6.15 with 1-μM FC in a 12-well plate to induce stomatal opening.

2.8 | COS^{488} Labeling and Immunolabeling

For COS^{488} labeling, 3- to 4-week-old rosette leaves were stained with COS^{488} diluted at 1:100 in ½ MS, pH 5.7, for 30 min, washed with and mounted in ½ MS media. A 488-nm excitation laser and a 525/550-nm emission filter were used for detection of COS^{488} signal. Fluorescence intensities of COS^{488} were quantified as described previously (Rui et al. 2017) with a region of interest defined in Figure 6a. Immunolabeling of guard cells was performed as described by Rui et al. (2017), with the following modifications. 3- to 4-week-old Arabidopsis rosette leaves of Col-0, *pme51-1*, *PME51-OE*, and *PME51-comp* plants were first trimmed into 3 × 3-mm squares and fixed in 4% paraformaldehyde in PEM buffer (0.1-M PIPES, 2-mM EGTA, and 1-mM MgSO4, pH 7.0) with vacuum infiltration for 1 h. Leaf cuts were then rinsed in PEM buffer, dehydrated in an ethanol series (25%, 50%, 70%, 80%, 85%, 90%, 95%, and 100% ethanol), and infiltrated with a series of LR White resin (a polyhydroxylated aromatic acrylic resin) (Electron Microscopy Sciences; 50, 75, and 100%) diluted in ethanol and incubated at 4°C for at least 4 h each. Samples were embedded vertically in 100% LR white resin in gelatin capsules (Ted Pella) and resin polymerization was performed at 60°C for 24 to 48 h. Thin sections (2 μm thick) were cut on a Leica UC6 ultramicrotome with a glass knife. For immunolabeling with LM19 (PlantProbes, University of Leeds; catalog no. LM19) and LM20 (PlantProbes; catalog no. LM20), sections were first blocked in KPBS buffer (0.01-M K3PO4 and 0.5-M NaCl, pH 7.1) with 3% BSA for at least 3 h. Sections were then incubated with a primary antibody at 1:10 dilution in KPBS buffer with 3% BSA at room temperature for 24 h in a humidified chamber. Samples were rinsed with KPBS buffer three times and incubated with Alexa Fluor 488-conjugated goat anti-rat IgG (H + L) (Jackson ImmunoResearch Laboratories; catalog no. 112-546-003) at 1:100 dilution in KPBS buffer with 3% BSA in the dark for 16 h. Sections were rinsed again with KPBS buffer three times before visualization. Images of immunolabeled sections were collected on a Zeiss Axio Observer microscope with a Yokogawa CSU-X1 spinning disk head and a 100 × 1.4 NA oil immersion objective, with a 488-nm excitation laser and a 525/550-nm emission filter for Alexa Fluor 488 signals. For a given primary antibody, the same settings of laser power, exposure time, and CCD gain values were always applied to both primary antibody-incubated sections and control sections across genotypes. Immunolabeling fluorescence intensities were analyzed as described previously (Chen et al. 2021). The ROIs selected for guard cells are as indicated in Figure 6f. Threshold function in ImageJ was used to select the areas with signal for quantification. The fluorescence intensity of each antibody was presented as a ratio of raw integrated density to area. The

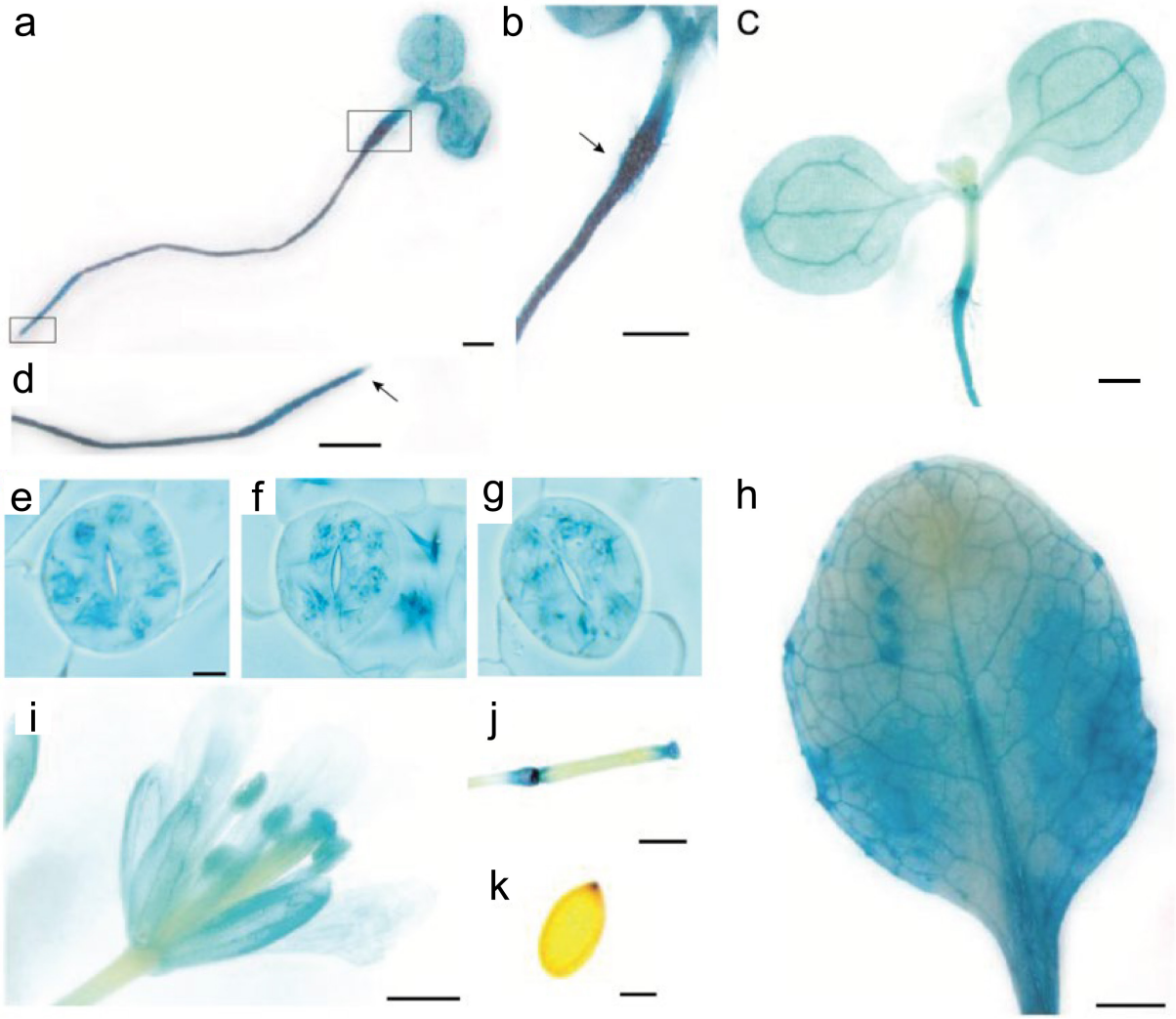

FIGURE 1 | The *PME51* promoter drives GUS expression throughout the plant, including in guard cells. (a–k) Images of GUS stained ProPME51::GUS transgenic plants. (a) Six-day-old light grown seedling; (b) close up view of 6-day-old hypocotyl; (c) close up view of 6-day-old cotyledons; (d) close up view of 6-day-old root tip. (e–g) Stomatal guard cells from 3-week-old rosette leaves; (h) 3-week-old rosette leaf; (i) 6-week-old flower; (j) silique from 6-week-old plant; (k) mature, dry seed. Scale bars are 1 mm for (a–d,i), 20 μm (e–g), 200 μm (h,k), and 100 μm (j).

fluorescence intensity in guard cell walls incubated without primary antibody was used as a negative control to subtract background fluorescence.

2.9 | Data Analysis

Image analysis was performed using FIJI software (FIJI). Statistical tests were performed using Prism 9 (Graphpad). ANOVA followed by Tukey's test were used to analyze data.

3 | Results

3.1 | *PME51* Is Widely Expressed in *A. thaliana*

Based on transcriptome data, *PME51* has been reported to be expressed in stomatal guard cells (Hachez et al. 2011). To examine the expression pattern of *PME51* in detail, we fused the upstream 2 kb preceding the *PME51* coding sequence to *β-GLUCURONIDASE* (*GUS*) and transformed this construct into Col-0 plants. GUS staining was evident in the roots (Figure 1a,b,d), and top and base of hypocotyls (Figure 1a,c) of 6-day-old seedlings, and in 3-week-old rosette leaves (Figure 1h). GUS staining in epidermal peels from 3-week-old leaves showed expression in guard cells (Figure 1e,f,g), but the gene is not guard cell-specific as some GUS activity was also seen in neighboring pavement cells. GUS signals were observed in localized regions of 6-week-old siliques (Figure 1j) but were not seen in mature seeds (Figure 1k). Thus, *PME51* is likely expressed widely across seedlings and adult plants, including in stomatal guard cells.

3.2 | Overexpression of *PME51* Results in a Smaller Exposed Rosette Leaf Area in Adult Plants

We next examined adult plant growth in a T-DNA line with an insertion in the first exon of *PME51* (SALK_069468, named *pme51-1*), a PME51 overexpression line where *PME51* expression was driven by the 35S promoter (*PME51-OE*), and a complementation line in which a construct containing the *PME51*

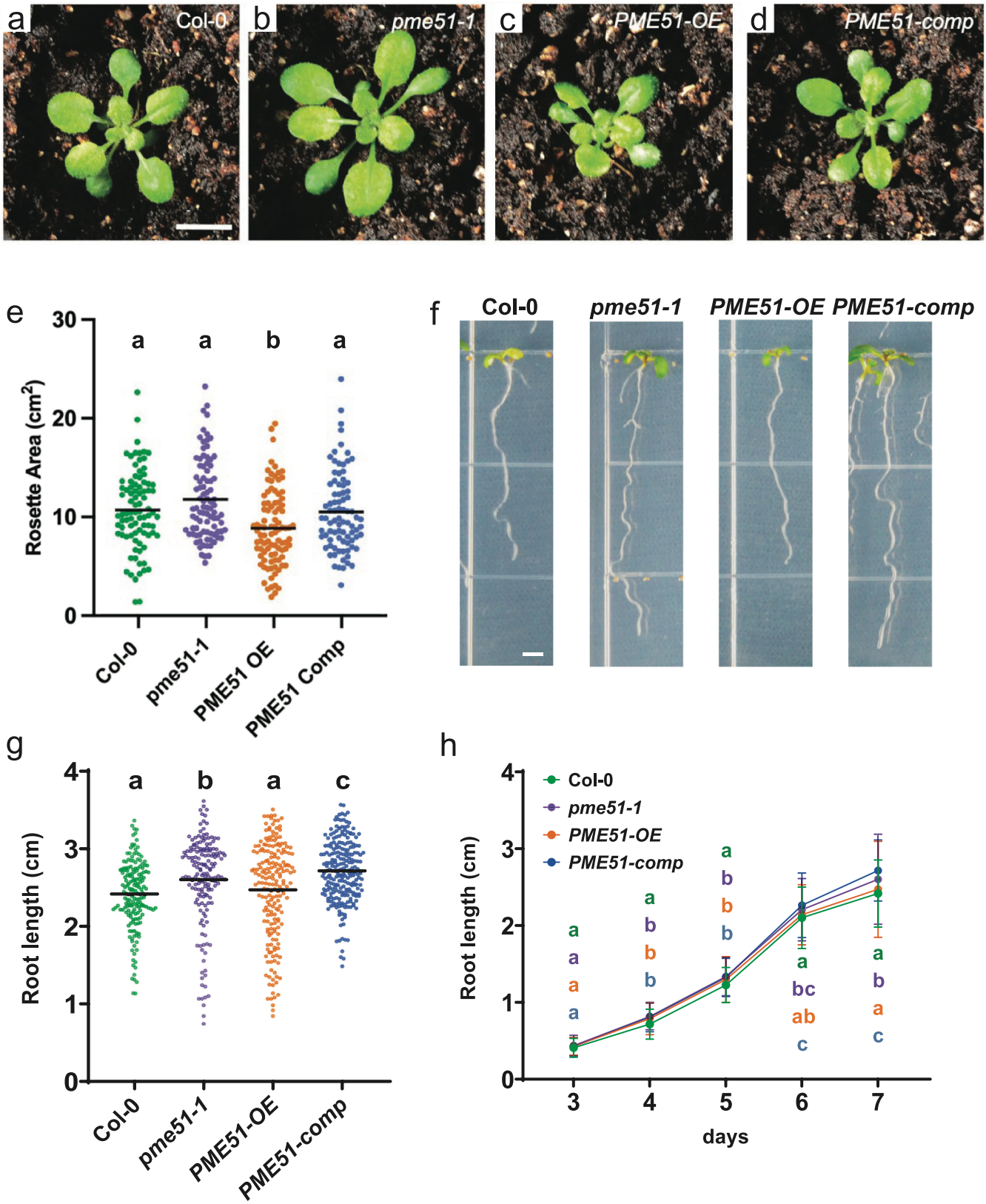

FIGURE 2 | Overexpressing *PME51* results in smaller rosettes whereas knocking out PME51 results in longer roots. (a–d) Representative images of 3-week-old *Arabidopsis thaliana* rosettes. Scale bar = 1 cm (a) Col-0; (b) *pme51-1*; (c) *PME51-OE*; (d) *PME51-comp*. (e) Measurements of average 3-week-old rosette area. (f) Representative images of 7-day old *A. thaliana* roots taken by Nikon D5100 camera. Scale bar is 0.25 cm. (g) Average root length in Col-0, *pme51-1*, *PME51-OE*, and *PME51-comp* lines in 7-day old *A. thaliana* seedlings and in (h) 3- to 7-day seedlings grown at 22°C under 24-h light conditions. Bars indicate mean across three independent experiments and letters represent significantly different groups ($n > 85$ plants per genotype); $p < 0.05$, ANOVA followed by Tukey's significance test.

CDS driven by a 2-kb region upstream of the *PME51* translational start site was transformed into the *pme51-1* background. Measuring the area of exposed rosette leaves (hereafter referred to as rosette area) in these lines and Col-0 controls showed that *PME51-OE* plants had significantly smaller rosette areas than Col-0 plants (Figure 2a,c,e). *pme51-1* and *PME51-comp* plants showed no significant difference in rosette area when compared with Col-0 plants (Figure 2a,d,e), although *pme51-1* plants had slightly larger rosette areas, (Figure 2a,b). Root length (Figure 2g,h) was also measured during the third through seventh day of growth of seedlings. As shown in Figure 2f–g, *pme51-1* seedlings had longer roots on day 7 than Col-0 controls. *PME51-OE* lines had similar root lengths to Col-0 seedlings whereas *PME51-comp* had the longest roots. Col-0 showed shortest roots until day 6 where both Col-0 and PME51-OE lines had similar roots lengths and by the day 7, *pme51-1* and *PME51-comp* roots showed significantly longer roots than both Col-0 and *PME51-OE* seedlings (Figure 2h). Overall, knocking out *PME51* leads to elongated roots but overexpressing *PME51* leads to reduction in the rosette area.

3.3 | Stomatal Pores Are Smaller in *pme51-1* Seedlings

Because *PME51* is expressed in stomatal guard cells, we next tested for differences in stomatal pore and complex size using propidium iodide staining of 6-day old Col-0, mutant and overexpression seedlings followed by confocal microscopy (Figure 3b–d). Plants were placed in light conditions for 2.5 h prior to staining to ensure that stomatal pores were open. In 6-day old cotyledons pore width, pore length, and pore/complex length ratio were smaller in *pme51-1* complexes than in Col-0 complexes (Figure 3e,f,h). When comparing *PME51-OE* to Col-0 complexes, there were no significant differences in pore and complex dimensions except for longer pore length in *PME51-OE* line (Figure 3f). These data indicate that loss of *PME51* inhibits the expansion of stomatal pores in seedling cotyledons.

3.4 | Stomatal Pores Are Shorter in Adult *pme51-1* Plants and Smaller in *PME51-OE* Plants

Because stomata might develop and function subtly differently in cotyledons versus true leaves, we next examined stomatal morphology in adult plants (Figure 4). Stomatal pores in *pme51-1* leaves had similar width as in Col-0 leaves, but *PME51-OE* pores were narrower than Col-0 pores (Figure 4a–e). Stomatal complexes in both *pme51-1* and *PME51-OE* leaves had smaller pore length, pore area, complex length and pore length: complex length ratio than in Col-0 complexes (Figure 4f–i). The smaller pore length: complex length ratio in 3-week-old *pme51-1* plants (Figure 4i) are consistent with the results found in 6-day-old plants (Figure 3h). In addition, pore length, pore area, complex length, and pore length:complex length ratio were all smaller in *PME51-OE* complexes than in Col-0 complexes in 3-week-old leaves (Figure 4), in contrast to 6-day-old seedlings where these values did not differ from Col-0 controls.

3.5 | *PME51-OE* Stomata Are More Closed at the Beginning of Stomatal Closure Assays and Show Faster Initial Responses to Light-Related Closure and Opening Stimuli

To examine the functional importance of *PME51* in modulating stomatal dynamics, stomatal responses were assessed using closing (abscisic acid, ABA, or dark) or opening (fusicoccin, FC, or light) assays in 3-week-old *A. thaliana* leaves across four different genotypes (Figure 5). *PME51-OE* and *PME51-comp* complexes had a smaller pore area immediately after the pre-incubation period of 2.5 h in light or dark, respectively, for both the closing and opening experiments (with the exception of light-induced opening) as compared with Col-0 and *pme51-1* complexes. However, by the end of the 120 min of exposure to ABA or FC, all genotypes had similar pore areas, with the exception of Col-0 stomatal pores being smaller after 120 min of light-induced opening (Figure 5d). We noted that *PME51-OE* complexes showed more rapid closure or opening in the first 30 min of light-related assays (Figure 5a–d). The rate of closure in the first 30 min for *PME51-OE* was $-0.00123\,\mu m^2$/min for dark-induced closure and $-0.00103\,\mu m^2$/min for Col-0. The rate of opening in the first 30 min for *PME51-OE* was $0.00647\,\mu m^2$/min for light-induced opening and $0.0034\,\mu m^2$/min for Col-0. Since the final pore areas in all genotypes were generally similar to those of Col-0 complexes, manipulation of *PME51* does not seem to significantly affect the limits of stomatal opening or closure but might affect the initial response rates of stomata to external stimuli.

3.6 | *PME51* Influences the Methylesterification Status of HG in Guard Cells

To probe demethylesterified HG and its distribution in guard cells as a function of *PME51* expression, we applied a chitosan-oligosaccharide-Alexa 488 probe, COS^{488}, which recognizes and binds to negatively charged carboxyl groups on stretches of demethylesterified GalA residues in HG (Mravec et al. 2014). COS^{488} was applied prior to immunolabeling because the immunolabeling procedure is incompatible with imaging intact cells. In contrast, COS^{488}, being a small molecule, can penetrate the cuticle, enabling labeling of intact guard cells without the need for fixation or sectioning. In our experiments, COS^{488}-labeled the walls of guard cells, with more fluorescence at guard cell junctions (Figure 6a–e). Quantification of COS^{488} labeling intensity in individual cells revealed that labeling in *pme51-1*, *PME51-OE*, and *PME51-comp* cells were significantly less intense than in Col-0 controls (Figure 6a–e,n), implying that less COS^{488} binding sites are present in those guard cell walls. To further validate the results from COS^{488} labeling, we also performed immunolabeling in cross sections of rosette leaves of 3- to 4-week-old Col, *pme51-1*, *PME51-OE*, and *PME51-comp* plants using antibodies that recognize different forms of HG (Figure 6f–m). LM19, which recognizes demethylesterified HG (Verhertbruggen et al. 2009); LM20, which recognizes methylesterified HG (Verhertbruggen et al. 2009). Our results indicated that LM19 labeled the guard cell surface more uniformly (Figure 6f–i), whereas LM20 showed more punctate labeling (Figure 6j–m). To quantify the differences in immunolabeling, we recorded the raw integrated density of

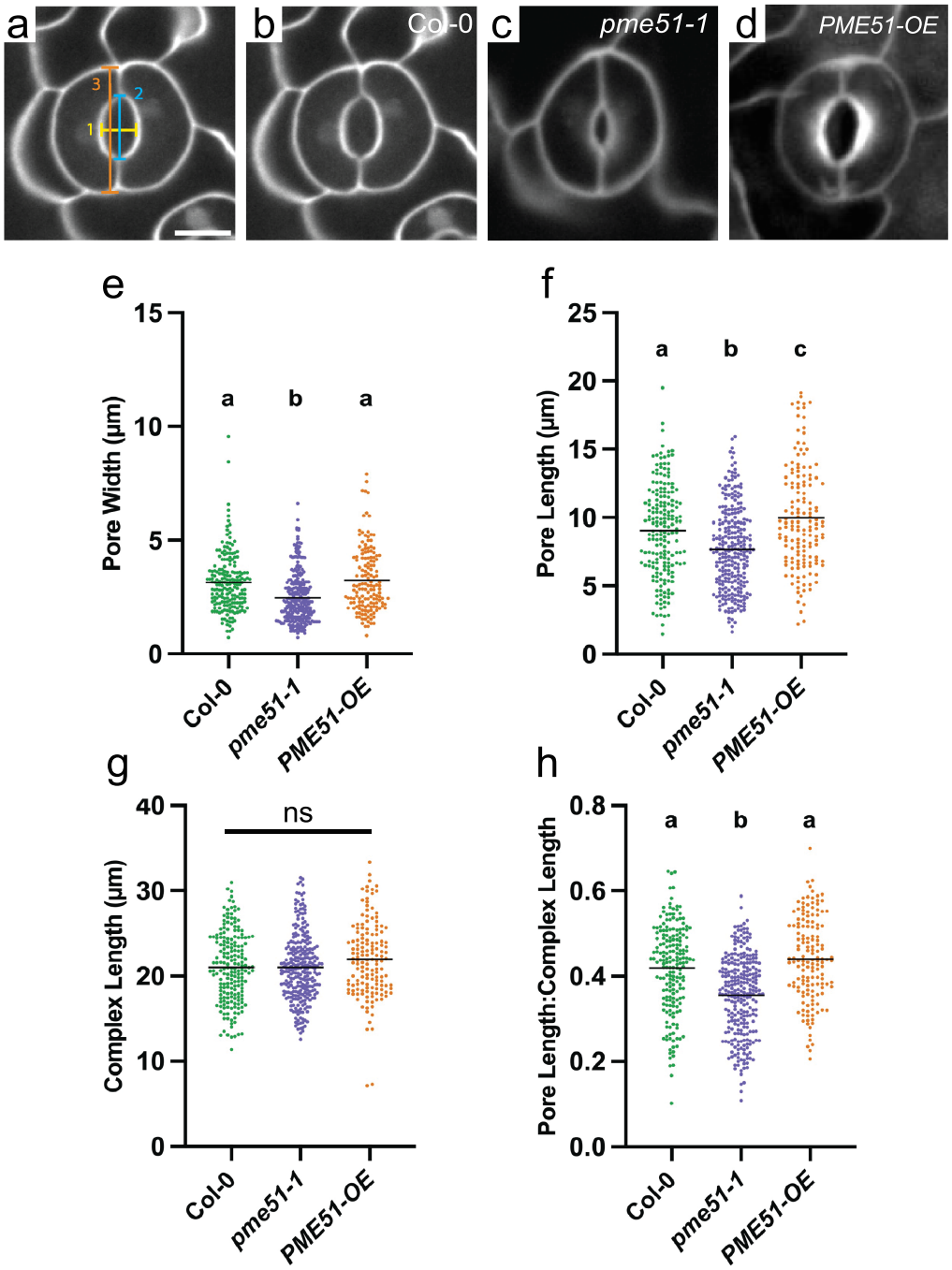

FIGURE 3 | *pme51-1* seedlings show smaller stomatal pores in cotyledons. (a) Representative image showing stomatal dimensions measured. Bracket 1 represents pore width, bracket 2 represents pore length, and bracket 3 represents complex length. Scale bar = 10 µm. (b–d) Representative images of PI stained 6-day-old cotyledons grown in 24-h light conditions. (e–h) Measurements of PI-stained stomata in 6-day-old light-grown seedlings: (e) pore width (bracket 1), (f) pore length (bracket 2), (g) complex length (bracket 3), and (h) pore length to complex length ratio (bracket 2/bracket 3). Bars indicate mean, and lowercase letters represent significantly different groups ($n > 120$ stomata per genotype from at least six seedlings per genotype across three independent experiments; $p < 0.05$, ANOVA followed by Tukey's statistical test).

fluorescence associated with the secondary antibody in each section, subtracted background autofluorescence from control sections (labeled with only the secondary antibody), and calculated the background-corrected intensity per area as an estimate of antibody labeling intensity (Figure 6o,p). However, based on LM19 labeling, we did not observe differences in the levels of low methyl-esterified HG across all four genotypes, unlike for the COS^{488} labeling results. (Figure 6f–i,o). On the other hand, PME51-OE showed significantly higher labeling with LM20 as compared with Col-0, *pme51-1*, and *PME51-comp* lines, indicating increased detection of methylesterified HG in *PME51-OE* (Figure 6j–m,p). This indicates that PME51 fine tunes the status of both methylesterified and demethylesterified HG in guard cell walls, providing a molecular explanation for the altered stomatal dynamics observed in PME51 knockout and overexpression plants.

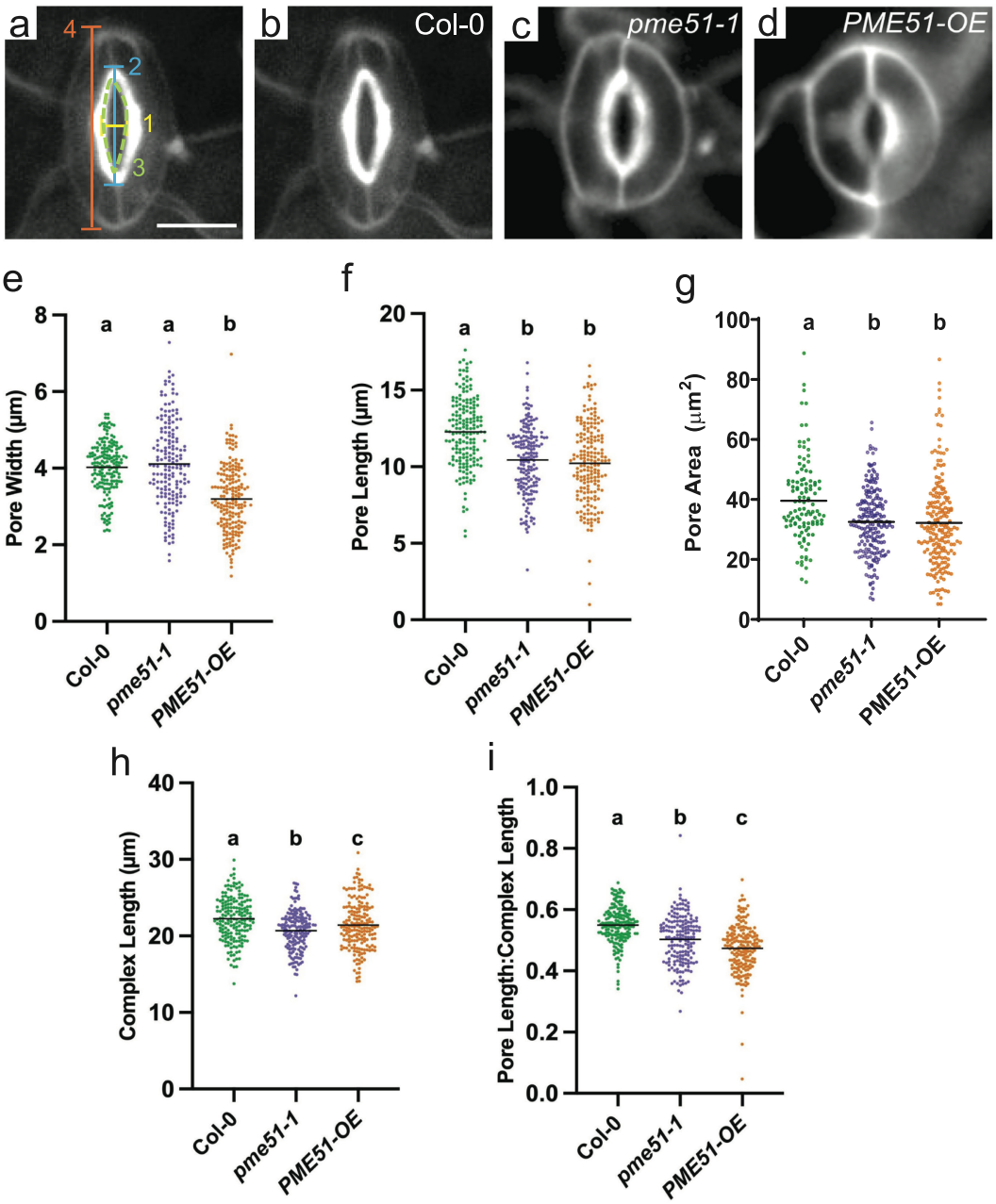

FIGURE 4 | Stomatal dimensions are abnormal in *pme51-1* and *PME51-OE* leaves. (a) Representative image showing stomatal dimensions measured. Scale bar = 10 µm. Bracket 1 represents pore width, bracket 2 represents pore length, bracket 3 represents pore area and bracket 4 represents complex length. (b–d) Representative images of PI stained 3-week-old *Arabidopsis thaliana* cotyledons grown in 24-h light conditions. (e–i) Measurements of 3-week-old light grown PI-stained Col-0, *pme51-1*, and *PME51-OE*. (e) pore width (bracket 1), (f) pore length (bracket 2), (g) pore area (bracket 3), (h) complex length (bracket 4), and (i) pore length to complex length ratio (bracket 2/4). Bars indicate mean, and lowercase letters represent significantly different groups. ($n > 120$ stomata from at least six seedlings per genotype across three independent experiments; $p < 0.05$, ANOVA followed by Tukey's statistical test).

4 | Discussion

In this study we characterized the expression pattern and functions of a putative pectin methylesterase, *PME51*, that is expressed in stomatal guard cells and more widely across other tissues (Figure 1). As shown in the rosette area data and representative images of 3-week-old plants (Figure 2a–e), *PME51-OE* plants have smaller rosette areas than Col-0, *pme51-1*, and *PME51-comp* plants. Conversely, knocking out *PME51* did not have significant effects on leaf expansion, potentially reflecting partial functional redundancy with other pectin methylesterases, although we did observe slightly larger leaves in *pme51-1* plants (Figure 2a,b). Based on these data we hypothesized that the more highly methylesterified state of HG in *pme51-1* plants might be less cross-linkable and cause the cell walls to be looser and more expandable, leading to larger rosettes, whereas more demethylesterified HG might enable cross-linking to stiffen the cell walls and inhibit cellular

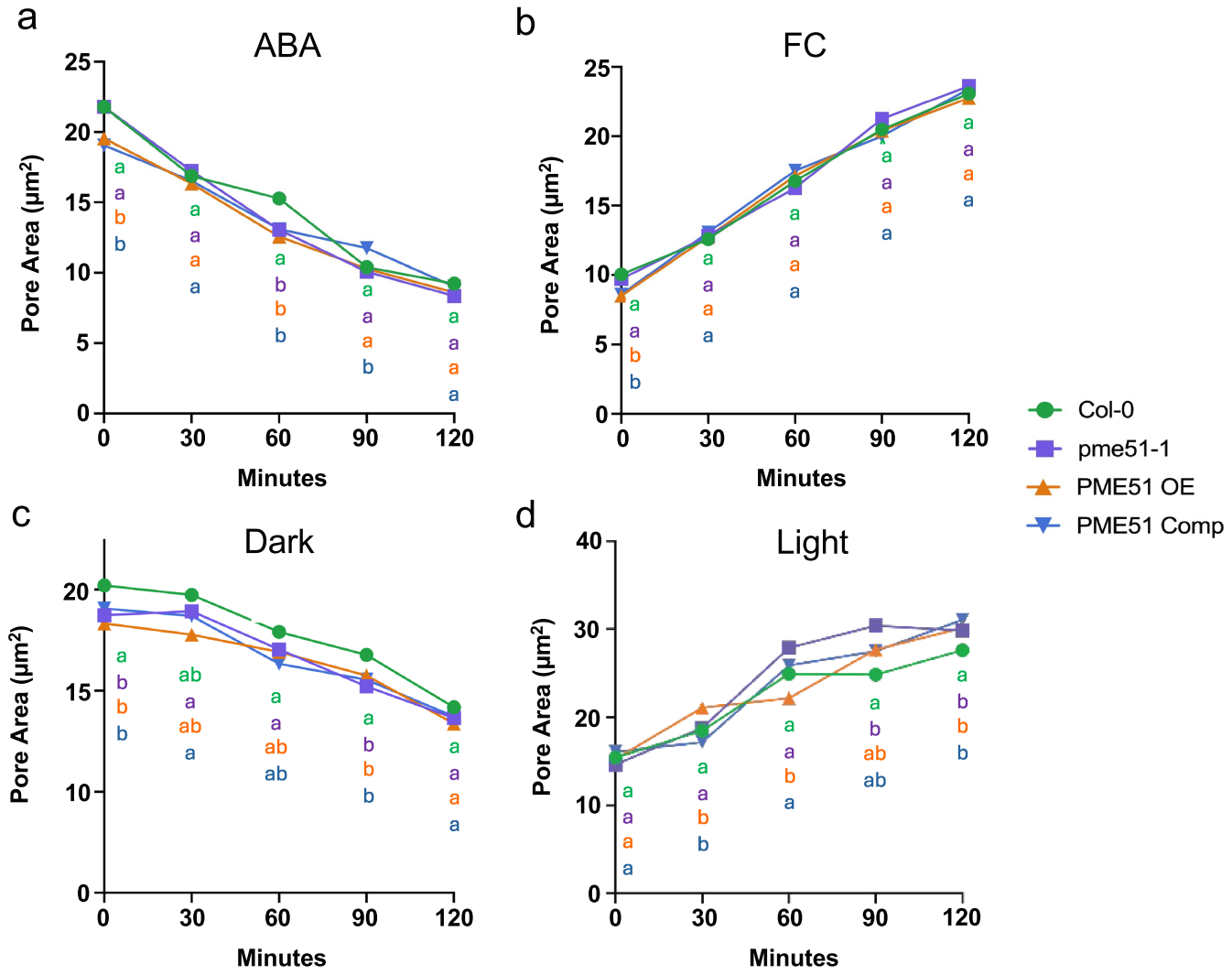

FIGURE 5 | *PME51-OE* stomata have smaller pore areas at the beginning of stomatal closure and opening assays. Graphs represent average pore areas of stomata in Col-0, *pme51-1*, *PME51-OE*, and *PME51-comp* of 3-week-old *Arabidopsis thaliana* plants over 120 min under ABA-induced closing (a), FC-induced opening (b), dark-induced closing (c), and light-induced opening (d) conditions. Images were collected with a 63X oil immersion objective on an epifluorescence microscope. $n > 120$ stomata per timepoint, nine plants per genotype across three independent experiments, $p < 0.05$, ANOVA statistical significance test followed by Tukey's test.

expansion in *PME51-OE* plants (Wu et al. 2018); however, our COS^{488}, LM19, and LM20 experiments indicated slightly contrasting results (Figure 6, S1). Our results indicate that in the absence of functional PME51, as seen in the *pme51-1* mutants, there was reduced COS^{488} staining, which aligns with the idea that less PME51 activity leads to fewer demethylesterified HG regions available for COS^{488} binding. Interestingly, in *PME51-OE* plants, we observed reduced COS^{488} staining but increased LM20 labeling, which suggests that higher PME51 activity might enable HG degradation, leaving a form of partially methylesterified HG in the cell wall material that may no longer be an accessible substrate for PME51 or pectinases, but is able to be bound by LM20. However, the precise LM20 epitope remains to be defined.

Seedling root lengths for *pme51-1* were longer than those of Col-0 and *PME51-OE* plants by the seventh day, but *PME51-OE* seedling roots were not smaller than those of Col-0 seedlings by the seventh day (Figure 2f,g). These data indicate that lack of *PME51* activity might lead to changes in the physical or signaling status of pectins that enhance the growth of roots. Our GUS staining results (Figure 1) show that *PME51* is expressed in the roots, however since *PME51-OE* root lengths did not significantly differ from Col-0, it is not evident that *PME51* plays a significant role in root elongation but may facilitate or moderate the functions of other PMEs in roots.

PI staining of stomatal complexes showed geometric differences across *PME51* genotypes as well as across developmental time. PI staining in 6-day-old *pme51-1* cotyledons showed smaller pore widths, pore lengths, and pore/complex length ratios than in Col controls (Figure 3). In addition to being important for pectin crosslinking, pectin methylesterase activity also makes HG susceptible to cleavage by polygalacturonases and pectase lyases (Peaucelle et al. 2012). The reduction in stomatal dimensions in *pme51-1* seedlings was similar to results for *pgx3* knockout seedlings, which lack a polygalacturonase and show a higher pectin molecular mass (Rui et al. 2017). Thus, the expansion of

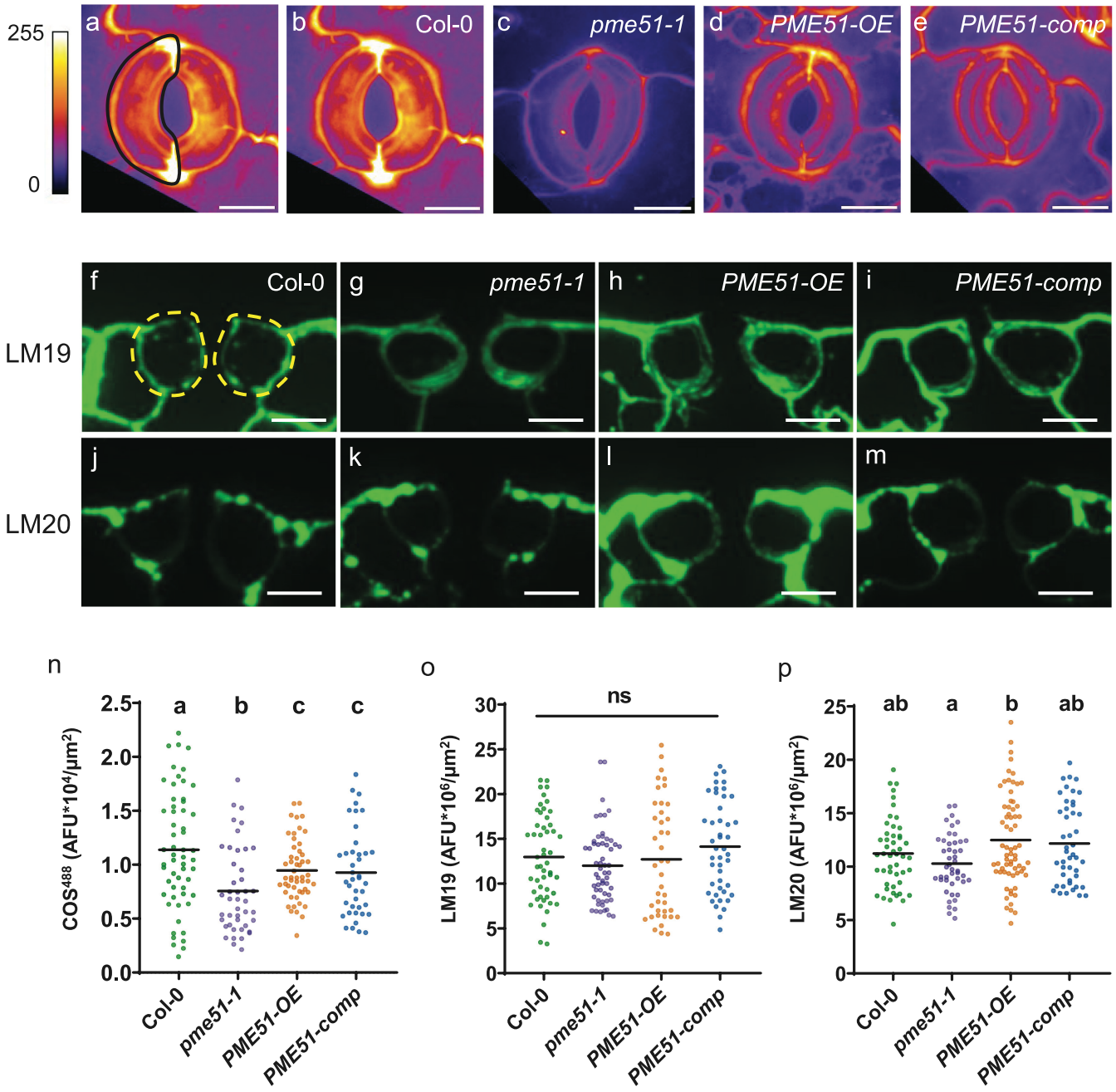

FIGURE 6 | *PME51* influences the methylesterification of HG in guard cells from true leaves. (a–e) COS^{488} labeling of guard cells. (a) shows representative maximum intensity projection of guard cells with ROIs indicated in black. Images are applied with fire look up table. Scale bars = 10 µm. (n) COS^{488} fluorescence intensities quantified in the walls of individual guard cells in 3- to 4-week-old Col, *pme51-1*, *PME51-OE*, and *PME51-comp* plants. (f–i) LM19 (top panel) and (j–m) LM20 (bottom panel) antibody labeling that recognize demethylesterified HG and methyesterified HG, respectively. Scale bars = 5 µm. (o,p) Fluorescence intensity quantifications of LM19 and LM20 labeling. Bars indicate mean, and lowercase letters represent significantly different groups. $n \geq 35$ guard cell pairs from three plants per genotype, three independent experiments; $p < 0.05$, one-way ANOVA and Tukey's test.

stomatal guard cells in seedlings might depend more on HG degradation than changes in HG crosslinking.

Stomatal complexes in 3-week-old *PME51-OE* plants exhibited smaller pore widths, pore length, pore area, complex lengths, and pore/complex length ratios compared with Col-0. This change in stomatal complex dimensions in the overexpression line might reflect stiffening of the cell walls in stomata that function more actively in soil-grown plants than in seedlings, which are grown in a water-rich environment. In adult plants, demethylesterification of HG might result in enhanced Ca^{2+} crosslinking, leading to wall stiffening (Limberg et al. 2000). However, neither our COS^{488} staining nor LM19/LM20 immunolabeling experiments support this hypothesis. We speculate that in the absence of PME51, pectin might be less susceptible to degradation by PGs/PLs, and this inhibits pore enlargement without affecting guard-cell size. In *PME51-OE* plants, the surviving pectin might be highly methylesterified (Figure 6j–m)

and therefore also less susceptible to degradation, resulting in smaller pores. However, the stronger signal observed in *PME51-OE* with LM20 labeling suggests that these methylesterification patterns may not be detectable by PME51 but are easily recognized by LM20 which recognizes methylesterified pectin, even in samples treated with pectin lyase, with an efficiency of about 66% (Verhertbruggen et al. 2009). A previous study (Rui et al. 2019) provides evidence for pectin degradation being important for pore formation/enlargement. However, it is unknown at this point what causes the observed difference in stomatal geometry between seedling and adult plants in the *PME51-OE* line. Possibly calcium cross-linking enabled by demethylesterification of HG is more predominant in 3-week-old *PME51-OE* plants and inhibits HG degradation and/or pore expansion. GUS staining (Figure 1) shows a higher expression of ProPME51:GUS in 3-week-old rosette leaves than in 6-day-old cotyledons. This correlates with the changes in stomatal dimensions shown in Figures 3 and 4.

Although the endpoints of stomatal opening or closure assays did not differ between *PME51* genotypes (Figure 5), stomatal complexes at the beginning of both the ABA and FC assays had smaller initial pore areas in *PME51-OE* plants, and thus the first phase of stomatal response differed from Col-0 controls. It is evident that *PME51* is expressed in the guard cells (Figure 1e–g) via GUS staining and that it might play a role in determining stomatal pore and complex dimensions (Figures 3 and 4); these effects should impinge on stomatal conductivity even when the ability of the guard cells to respond to opening or closing stimuli is not compromised. Additionally, enhanced PME activity in the *PME51-OE* plants might tune the response mechanics of these guard cells to make them more flexible during the initial stages of stomatal opening, in a way that differs from the effects of *PME51* overexpression on guard cell growth. The effects of *PME51* on stomatal conductance might not show differences over this 2-h period, but the rapidity of stomatal response is an important determinant of water use efficiency in plants (Lawson and Vialet-Chabrand 2019); future whole-plant physiological measurements and mechanical analyses of guard cell walls (Chen et al. 2021; Keynia et al. 2023) in different *PME51* genotypes could be performed to test this idea. Under dark and light conditions, stomatal pores in all genotypes were closed more slowly compared with ABA-induced closure. As found in Figure 5, *PME51-OE* complexes experienced more rapid stomatal responses. *PME51-OE* complexes were found to be smaller than the other genotypes. Smaller stomata have been found to have faster changes in stomatal conductance, which might explain why these stomata respond more in the first 30 min of assays (Drake et al. 2013).

In summary, the above data demonstrate that *PME51* inhibits plant growth when overexpressed, functions in stomatal morphogenesis, and has a subtle influence on stomatal dynamics. Further physiological and biomechanical studies and analyses of cell wall structure and pectin status could provide more detail regarding the impacts of this gene on stomatal development and function, as well as whole-plant growth. It will also be interesting to study the effects of *PME51* orthologs on stomatal function in other plant species to expand our knowledge of how pectin demethylesterification modulates the properties of the plant cell wall to tune stomatal responses.

Author Contributions

AD, RM, and CTA conceptualized and designed the experiments. AD, RM, and CT performed the experiments and analyzed the data. AD, RM, CT, and CTA wrote the manuscript.

Acknowledgments

The authors would like to thank Taylor Purzycki for the foundational work on this project and Yintong Chen, Leila Jaafar, Ellen Zelinsky, and other members of the Anderson Laboratory for helpful discussions. This work was supported by the National Science Foundation under grant MCB-2015943/2015947.

Conflicts of Interest

The authors declare no conflicts of interest.

Data Availability Statement

The data that support the findings of this study are available from the corresponding author upon reasonable request.

Peer Review

The peer review history for this article is available in the Supporting Information for this article.

References

Amsbury, S., L. Hunt, N. Elhaddad, et al. 2016. "Stomatal Function Requires Pectin De-Methyl-Esterification of the Guard Cell Wall." *Current Biology* 26, no. 21: 2899–2906. https://doi.org/10.1016/j.cub.2016.08.021.

Bosch, M., and P. K. Hepler. 2006. "Silencing of the Tobacco Pollen Pectin Methylesterase NtPPME1 Results in Retarded In Vivo Pollen Tube Growth." *Planta* 223, no. 4: 736–745. https://doi.org/10.1007/s00425-005-0131-x.

Caffall, K. H., and D. Mohnen. 2009. "The Structure, Function, and Biosynthesis of Plant Cell Wall Pectic Polysaccharides." *Carbohydrate Research* 344, no. 14: 1879–1900. https://doi.org/10.1016/j.carres.2009.05.021.

Chen, Y., W. Li, J. A. Turner, and C. T. Anderson. 2021. "PECTATE LYASE LIKE12 Patterns the Guard Cell Wall to Coordinate Turgor Pressure and Wall Mechanics for Proper Stomatal Function in Arabidopsis." *Plant Cell* 33, no. 9: 3134–3150. https://doi.org/10.1093/plcell/koab161.

Drake, P. L., R. H. Froend, and P. J. Franks. 2013. "Smaller, Faster Stomata: Scaling of Stomatal Size, Rate of Response, and Stomatal Conductance." *Journal of Experimental Botany* 64, no. 2: 495–505. https://doi.org/10.1093/jxb/ers347.

Earley, K. W., J. R. Haag, O. Pontes, et al. 2006. "Gateway-Compatible Vectors for Plant Functional Genomics and Proteomics." *Plant Journal* 45, no. 4: 616–629. https://doi.org/10.1111/j.1365-313X.2005.02617.x.

Hachez, C., K. Ohashi-Ito, J. Dong, and D. C. Bergmann. 2011. "Differentiation of Arabidopsis Guard Cells: Analysis of the Networks Incorporating the Basic Helix-Loop-Helix Transcription Factor, FAMA." *Plant Physiology* 155, no. 3: 1458–1472. https://doi.org/10.1104/pp.110.167718.

Harholt, J., A. Suttangkakul, and H. Vibe Scheller. 2010. "Biosynthesis of Pectin." *Plant Physiology* 153, no. 2: 384–395. https://doi.org/10.1104/pp.110.156588.

Jones, L., J. L. Milne, D. Ashford, and S. J. McQueen-Mason. 2003. "Cell Wall Arabinan Is Essential for Guard Cell Function." *Proceedings of the National Academy of Sciences* 100, no. 20: 11783–11788. https://doi.org/10.1073/pnas.1832434100.

Keynia, S., L. Jaafar, Y. Zhou, C. T. Anderson, and J. A. Turner. 2023. "Stomatal Opening Efficiency Is Controlled by Cell Wall Organization in *Arabidopsis thaliana*." *PNAS Nexus* 2, no. 9: pgad294. https://doi.org/10.1093/pnasnexus/pgad294.

Kim, T.-H., M. Böhmer, H. Hu, N. Nishimura, and J. I. Schroeder. 2010. "Guard Cell Signal Transduction Network: Advances in Understanding Abscisic Acid, CO_2, and Ca^{2+} Signaling." *Annual Review of Plant Biology* 61, no. 1: 561–591. https://doi.org/10.1146/annurev-arplant-042809-112226.

Lawson, T., and S. Vialet-Chabrand. 2019. "Speedy Stomata, Photosynthesis and Plant Water Use Efficiency." *New Phytologist* 221, no. 1: 93–98. https://doi.org/10.1111/nph.15330.

Limberg, G., R. Körner, H. C. Buchholt, T. M. I. E. Christensen, P. Roepstorff, and J. D. Mikkelsen. 2000. "Analysis of Different De-Esterification Mechanisms for Pectin by Enzymatic Fingerprinting Using Endopectin Lyase and Endopolygalacturonase II From *A. Niger*." *Carbohydrate Research* 327, no. 3: 293–307. https://doi.org/10.1016/S0008-6215(00)00067-7.

Liners, F., J.-J. Letesson, C. Didembourg, and P. Van Cutsem. 1989. "Monoclonal Antibodies Against Pectin." *Plant Physiology* 91, no. 4: 1419–1424. https://doi.org/10.1104/pp.91.4.1419.

Liu, H., S. Song, H. Zhang, et al. 2022. "Signaling Transduction of ABA, ROS, and Ca^{2+} in Plant Stomatal Closure in Response to Drought." *International Journal of Molecular Sciences* 23, no. 23: 14824. https://doi.org/10.3390/ijms232314824.

Manmohit Kalia, P. K. 2015. "Pectin Methylesterases: A Review." *Journal of Bioprocessing & Biotechniques* 05, no. 05: 1000227. https://doi.org/10.4172/2155-9821.1000227.

Micheli, F. 2001. "Pectin Methylesterases: Cell Wall Enzymes With Important Roles in Plant Physiology." *Trends in Plant Science* 6, no. 9: 414–419. https://doi.org/10.1016/S1360-1385(01)02045-3.

Mravec, J., S. K. Kračun, M. G. Rydahl, et al. 2014. "Tracking Developmentally Regulated Post-Synthetic Processing of Homogalacturonan and Chitin Using Reciprocal Oligosaccharide Probes." *Development* 141: 4841–4850. https://doi.org/10.1242/dev.113365.

Peaucelle, A., S. Braybrook, and H. Höfte. 2012. "Cell Wall Mechanics and Growth Control in Plants: The Role of Pectins Revisited." *Frontiers in Plant Science* 3: 121. https://doi.org/10.3389/fpls.2012.00121.

Rui, Y., C. Xiao, H. Yi, et al. 2017. "POLYGALACTURONASE INVOLVED IN EXPANSION3 Functions in Seedling Development, Rosette Growth, and Stomatal Dynamics in *Arabidopsis thaliana*." *Plant Cell* 29, no. 10: 2413–2432. https://doi.org/10.1105/tpc.17.00568.

Rui, Y., Y. Chen, H. Yi, T. Purzycki, V. M. Puri, and C. T. Anderson. 2019. "Synergistic Pectin Degradation and Guard Cell Pressurization Underlie Stomatal Pore Formation." *Plant Physiology* 180: 66–77. https://doi.org/10.1104/pp.19.00135.

Sénéchal, F., L. Graff, O. Surcouf, et al. 2014. "Arabidopsis PECTIN METHYLESTERASE17 Is Co-Expressed With and Processed by SBT3.5, a Subtilisin-Like Serine Protease." *Annals of Botany* 114, no. 6: 1161–1175. https://doi.org/10.1093/aob/mcu035.

Verhertbruggen, Y., S. E. Marcus, A. Haeger, J. J. Ordaz-Ortiz, and J. P. Knox. 2009. "An Extended Set of Monoclonal Antibodies to Pectic Homogalacturonan." *Carbohydrate Research* 344: 1858–1862. https://doi.org/10.1016/j.carres.2008.11.010.

Wolf, S., T. Rausch, and S. Greiner. 2009. "The N-Terminal Pro Region Mediates Retention of Unprocessed Type-I PME in the Golgi Apparatus." *Plant Journal* 58, no. 3: 361–375. https://doi.org/10.1111/j.1365-313X.2009.03784.x.

Wu, H.-C., V. P. Bulgakov, and T.-L. Jinn. 2018. "Pectin Methylesterases: Cell Wall Remodeling Proteins Are Required for Plant Response to Heat Stress." *Frontiers in Plant Science* 9: 1612. https://doi.org/10.3389/fpls.2018.01612.

Wu, H.-C., Y.-C. Huang, L. Stracovsky, and T.-L. Jinn. 2017. "Pectin Methylesterase Is Required for Guard Cell Function in Response to Heat." *Plant Signaling & Behavior* 12, no. 6: e1338227. https://doi.org/10.1080/15592324.2017.1338227.

Zablackis, E., J. Huang, B. Muller, A. G. Darvill, and P. Albersheim. 1995. "Characterization of the Cell-Wall Polysaccharides of *Arabidopsis thaliana* Leaves." *Plant Physiology* 107, no. 4: 1129–1138. https://doi.org/10.1104/pp.107.4.1129.

Supporting Information

Additional supporting information can be found online in the Supporting Information section.